Topological superconductivity in Landau levels

Gun Sang Jeon, J. K. Jain, and C.-X. Liu

Topological superconductivity in Landau levels

Gun Sang Jeon[1,2], J. K. Jain[1], C.-X. Liu[1]

[1]*Department of Physics, 104 Davey Lab, The Pennsylvania State University, University Park, Pennsylvania 16802 and*
[2]*Department of Physics, Ewha Womans University, Seoul 03760, Korea*
(Dated: January 7, 2019)

The intense search for topological superconductivity is inspired by the prospect that it hosts Majorana quasiparticles. We explore in this work the optimal design for producing topological superconductivity by combining a quantum Hall state with an ordinary superconductor. To this end, we consider a microscopic model for a topologically trivial two-dimensional p-wave superconductor exposed to a magnetic field, and find that the interplay of superconductivity and Landau level physics yields a rich phase diagram of states as a function of μ/t and Δ/t, where μ, t and Δ are the chemical potential, hopping strength, and the amplitude of the superconducting gap. In addition to quantum Hall states and topologically trivial p-wave superconductor, the phase diagram also accommodates regions of topological superconductivity. Most importantly, we find that application of a non-uniform, periodic magnetic field produced by a square or a hexagonal lattice of h/e fluxoids greatly facilitates regions of topological superconductivity in the limit of $\Delta/t \to 0$. In contrast, a uniform magnetic field, a hexagonal Abrikosov lattice of $h/2e$ fluxoids, or a one dimensional lattice of stripes produces topological superconductivity only for sufficiently large Δ/t.

I. INTRODUCTION

Quasiparticle excitations in certain two dimensional (2D) condensed matter systems can possess exotic anyonic statistics that are fundamentally different from the familiar bosonic and fermionic statistics[1,2]. One example of such quasiparticle excitations is the Majorana zero mode (MZM)[3–5], which obeys non-Abelian statistics and has motivated ideas on topological quantum computation[2,6–8]. MZM can appear as a gapless quasiparticle excitation at the boundary or inside the vortex core of a topological superconductor (TSC). Intensive experimental effort has focused on the realization of TSC and the measurement of MZMs and their non-Abelian statistics in a variety of systems, including 5/2 fractional quantum Hall (QH) state[9] (which can be viewed as a TSC of composite fermions), p-wave Sr_2RuO_4 superconductors (SCs)[10], semiconductor nanowires in proximity to SCs under magnetic fields[11–17], magnetic ion chains on top of SC substrates[18], the surface of $(Bi,Sb)_2Te_3$ in proximity to SCs[19–21], the surface of Fe(Se,Te) SCs[22–25] and the heterostructure with a quantum anomalous Hall (QAH) insulator coupled to a SC[26–28]. In the last case, the interpretation of a recent report of TSC phase[28] is under debate[29–31]. Proposals have been made for demonstrating Majorana braiding and non-Abelian statistics through coherent transport measurement (interferometry) in the QAH-SC hybrid systems[32].

There are compelling reasons for pursuing TSC phase induced by coupling a QH state with a topologically trivial SC. First of all, while QAH has so far been seen by very few groups and requires stringent experimental conditions, QH effect is routinely observed all over the world in many different materials, which offers much flexibility in coupling it to superconductivity; indeed, several papers have reported supercurrent and Andreev reflection in this system[33–37]. Second, the QAH systems are typically highly disordered with low mobilities due to magnetic doping[38]. In contrast, very high mobilities can be achieved for QH samples. The resulting long coherence lengths can be a crucial factor for the success of interference measurements that can possibly verify braiding of emergent anyons. Third, because of higher Landau levels (LLs), the QH system offers additional structure without analog in QAH insulators. Finally, it opens the door into even more exotic particles that appear due to coupling between fractional QH effect and superconductivity. It therefore appears surprising that, to our knowledge, no experiment has made a serious attempt to produce TSC by coupling QH state with a topologically trivial SC. One reason is that for coupling between QH state and SC, it would be necessary for superconductivity to contain a non-zero p-wave triplet component, and also to survive to magnetic fields that are sufficiently high to bring the system into QH regime. This difficulty is currently surmountable, as discussed below. We believe that an important reason why experimental efforts have not been made is the absence of realistic proposals. That is the primary motivation for our study. We find that the most serious conceptual impediment in establishing an effective coupling between a SC and a QH state is that the latter is gapped and thus robust to small perturbations, making it impervious to coupling with weak superconductivity. A crucial message of our work is that one may circumvent this problem by considering spatially non-uniform magnetic fields, which produces "dispersive" LLs and supports gapless states for appropriate chemical potentials. We further find that the feasibility of TSC depends also on the magnetic flux lattice structure, and identify which geometries are most hospitable to TSC in the weak coupling limit.

The topological character of the states of interest to us will be quantified by the Chern number. The QH state has Chern number $\mathcal{C} =$integer, which corresponds to the number of LLs below the chemical potential. We will use the Bogoliubov-de Gennes (BdG) framework to enable a

treatment of superconductivity. In the BdG formulation, we can define another Chern number $\mathcal{N}$, defined below, which is called SC Chern number. In the zero SC gap limit, a QH state has $\mathcal{N} = 2\mathcal{C}$ due to the redundancy of the BdG Hamiltonian. Therefore, any state with even $\mathcal{N}$ is equivalent to a QH state with $\mathcal{C} = \mathcal{N}/2$ and not of interest to us. We define below the states with odd integer values of $\mathcal{N}$ as the TSC states. Such a state should possess an odd number of chiral Majorana modes at the boundary and odd number of MZMs trapped at the core of a vortex. Non-Abelian statistics for the vortex is only possible for a state with odd $\mathcal{N}$.

In what follows, we explore a microscopic model of 2D spinless electron system with nearest-neighbor SC pairing subjected to a magnetic field, and obtain the phase diagram of various states as a function of the chemical potential (μ), the hopping strength (t) and magnitude of the superconducting gap (Δ). For a uniform magnetic field, we find, as expected, that a TSC phase requires the strength of the superconducting coupling to be enhanced beyond a critical value to overcome the QH gap. We therefore consider non-uniform magnetic fields, which still produce LLs, but the LLs are dispersive (rather than flat). The most natural model, that of an Abrikosov lattice of $h/2e$ fluxoids, fails to produce TSC for small Δ/t (see App. D). In contrast, a square lattice of h/e fluxoids produces an enormously rich phase diagram with many regions of TSC with various odd $\mathcal{N}$. Most importantly, even a weak p-wave superconductor ($\Delta/t \to 0$) can turn into a TSC for appropriate chemical potentials. We have also considered a geometry where the magnetic field forms stripes; this geometry fails to produce TSC for small Δ/t. Our calculations thus provide insight into how best to integrate SC gap with LLs to realize TSC. We also discuss possible experimental manifestations.

II. MODEL HAMILTONIAN

We have in mind a general flux lattice, which can possibly be realized through a hybrid of 2D electron gas with p-wave SC grid on top exposed to an external magnetic field [Fig. 1(a)]. (The p-wave SC grid serves a dual purpose: it induces superconductivity and also produces a magnetic flux lattice.) We model such a hybrid system through spinless fermions on a square lattice in the presence of nearest-neighbor pairing and a perpendicular magnetic field. (The lattice represents the continuum in the limit of vanishing lattice spacing. We have confirmed, as elaborated in App. C, that the results presented below provide a good qualitative and semi-quantitative approximation of the continuum limit.) One unit cell consists of $N \times N$ lattice sites with lattice spacing a_1, as shown in Fig. 1(b) and (c). We next show results for a uniform magnetic field as well as for several kinds of flux lattices. In the first configuration, depicted in Fig. 1(b), single flux quanta (h/e) of a square shape are located in an $M \times M$ square at the center of each unit cell. Fig-
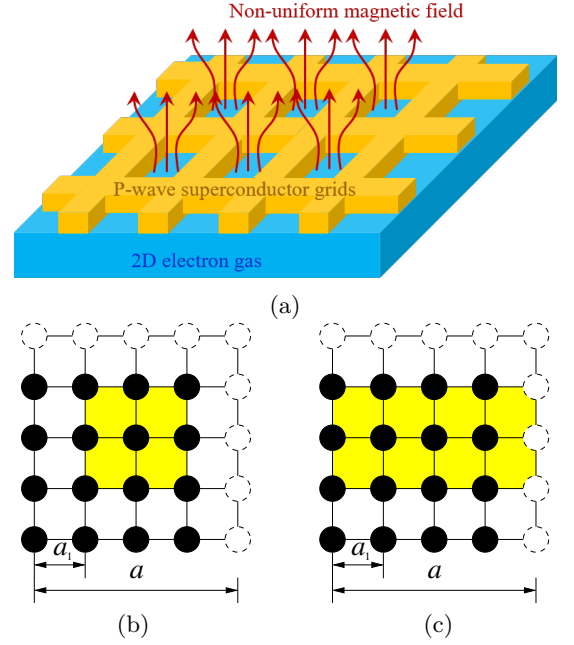

FIG. 1. (a) Experimental setup for a hybrid system with two-dimensional electron gas with p-wave superconducting grid on top under an external magnetic field. (b-c) Schematic of a unit cell of $N \times N$ lattice points containing one flux quantum (b) of a square shape; (c) in stripe geometry. In each unit cell a flux quantum ϕ_0 penetrates through the yellow shaded zone of (b) $M \times M$ (c) $N \times M$ lattice points. The figures represent $N = 4$ and $M = 2$. The size of unit cell is a and spacing between lattice points is $a_1 = a/N$.

ure 1(c) shows single flux quanta in an $N \times M$ rectangle in each unit cell, producing periodic stripes of magnetic field. In both configurations $M = N$ gives uniformly distributed magnetic field. (It is noted that the h/e flux quantum must have a finite extent to have an effect; a point flux quantum may be gauged away.) The lattice periodicity is $a = Na_1$ and the lattice vector is decomposed as $\boldsymbol{r_{i=(i_x,i_y)}} = \boldsymbol{R_{m=(m_x,m_y)}} + \boldsymbol{\tilde{r}_{l=(l_x,l_y)}}$ for $(i_x, i_y) = (Nm_x + l_x, Nm_y + l_y)$ with $0 \leq l_{x/y} < N$, $0 \leq m_{x/y} < L$, and La being the linear size of the system. Here, $\boldsymbol{R_m}$ represents the position of the reference point in the $\boldsymbol{m}$th unit cell and $\boldsymbol{\tilde{r}_l}$ is the internal position relative to $\boldsymbol{R_m}$.

The full Hamiltonian with nearest neighbor pairing on the lattice is given by

$$\mathcal{H} = -t \sum_{\boldsymbol{j,\delta}} (e^{iA_{\boldsymbol{j+\delta,j}}} c^{\dagger}_{\boldsymbol{j+\delta}} c_{\boldsymbol{j}} + e^{iA_{\boldsymbol{j,j+\delta}}} c^{\dagger}_{\boldsymbol{j}} c_{\boldsymbol{j+\delta}})$$
$$- \mu \sum_{\boldsymbol{i}} c^{\dagger}_{\boldsymbol{i}} c_{\boldsymbol{i}} - \Delta \sum_{\boldsymbol{j,\delta}} (c_{\boldsymbol{j+\delta}} c_{\boldsymbol{j}} + c^{\dagger}_{\boldsymbol{j}} c^{\dagger}_{\boldsymbol{j+\delta}}) \quad (1)$$

where $c_{\boldsymbol{i}}$ ($c^{\dagger}_{\boldsymbol{i}}$) annihilates (creates) a spinless electron at $\boldsymbol{r_i}$; $\boldsymbol{\delta} = (1,0), (0,1)$; $A_{\boldsymbol{j,j'}} = -A_{\boldsymbol{j',j}}$; and

$$\sum_{P} A_{\boldsymbol{j,j'}} = \begin{cases} 2\pi f & \text{inside a flux} \\ 0 & \text{otherwise} \end{cases} \quad (2)$$
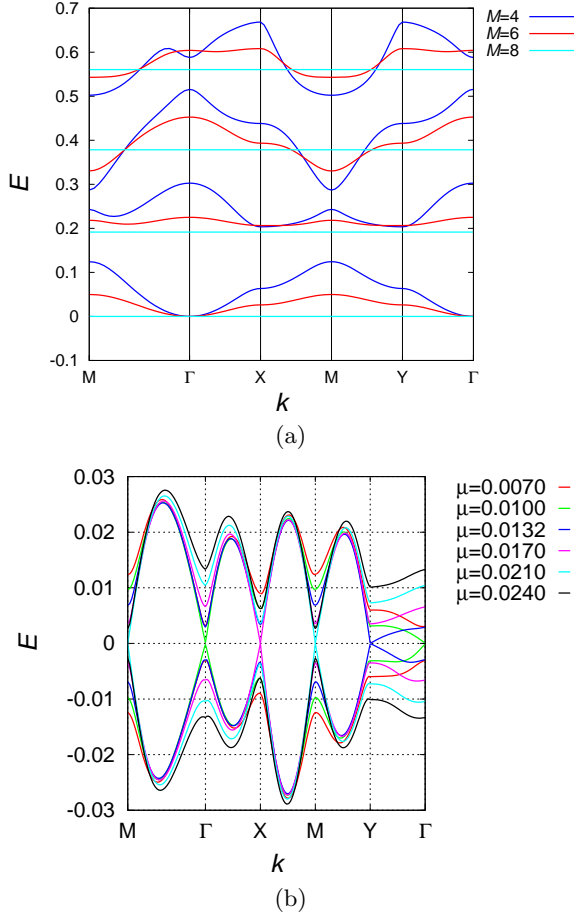
FIG. 2. (a) Energy dispersion in the presence of uniform magnetic field ($M = 8$) and non-uniform magnetic fields ($M = 4, 6$) for $N = 8$ and $\Delta = 0$. (b) Energy dispersion near the Fermi energy for various values of chemical potential μ in the presence of uniform magnetic field ($M = 8$) with $N = 8$ and $\Delta = 0.1$.

with P denoting a directional plaquette sum and $f \equiv 1/N_P$. Here N_P is the number of plaquettes though which fluxes penetrate in one unit cell. ($N_P = M^2$ for square-shape flux and $N_P = NM$ for stripe flux.) With $c_i = \frac{1}{L} \sum_{\boldsymbol{k}} e^{i\boldsymbol{k}\cdot\boldsymbol{R_m}} c_{\boldsymbol{k},\tilde{\boldsymbol{r}_l}}$, where $|k_x| \leq \pi/a, |k_y| \leq \pi/a$, we can transform the Hamiltonian into the BdG form on the basis $\boldsymbol{C}_{\boldsymbol{k}}^{\dagger} \equiv (c_{\boldsymbol{k},\tilde{\boldsymbol{r}}_{(0,0)}}^{\dagger}, \dots, c_{\boldsymbol{k},\tilde{\boldsymbol{r}}_{(N-1,N-1)}}^{\dagger}, c_{-\boldsymbol{k},\tilde{\boldsymbol{r}}_{(0,0)}}, \dots, c_{-\boldsymbol{k},\tilde{\boldsymbol{r}}_{(N-1,N-1)}})$. The detailed matrix elements are given in App. A. The numerical diagonalization of the BdG Hamiltonian gives $2N^2$ bands of eigen-energies $E_{n,\boldsymbol{k}}$ with the eigenvectors $|n,\boldsymbol{k}\rangle$ with $n = 1, 2, \dots, 2N^2$. The SC Chern number $\mathcal{N}$

can be computed by[26,39]

$$\mathcal{N} = \frac{1}{\pi} \int d^2\boldsymbol{k} \sum_{n=1}^{N^2} \sum_{m(\neq n)}^{2N^2}$$

$$\frac{\mathrm{Im}\langle m,\boldsymbol{k}|(\partial_{\boldsymbol{k}_x}\mathcal{H}_{\boldsymbol{k}})|n,\boldsymbol{k}\rangle^* \langle m,\boldsymbol{k}|(\partial_{\boldsymbol{k}_y}\mathcal{H}_{\boldsymbol{k}})|n,\boldsymbol{k}\rangle}{(E_{n,\boldsymbol{k}} - E_{m,\boldsymbol{k}})^2},$$

(3)

and identifies each topological phase in the phase diagram. The Chern number $\mathcal{N}$ changes at the boundaries of two distinct phases where the energy gap closes at some momentum. Henceforth, the energy is expressed in units of t. (Note that we have defined the SC Chern number with respect to half of the bands, rather than with respect to occupied states below the chemical potential. In cases where the chemical potential lies inside a gap, the two definitions coincide. We also find some semi-metallic regions, shown in App. B, where this is not the case.)

III. TSC PHASE AND PHASE DIAGRAM

The energy dispersion of our model Hamiltonian without superconductivity ($\Delta = 0$) is shown in Fig. 2a for different magnetic flux sizes M. A uniformly distributed magnetic field ($M = N$) yields flat Landau levels (cyan lines in Fig. 2a). For non-uniform magnetic fields, Landau levels turn into dispersive "Landau" bands (blue and red lines in Fig. 2a). The Chern number $\mathcal{C}$ carried by each band is unchanged since there is no level crossing between different bands. Due to the dispersive bands, the Fermi surface can appear and the system becomes metallic for certain ranges of μ, in contrast to the insulating phase of filled Landau levels obtained for a uniform magnetic field. A SC gap can be opened by turning on Δ. By varying the Fermi energy, multiple Dirac type of transitions are found, indicating the existence of topological phase transitions. In Fig.2b, we plot variation of energy dispersions for several values of chemical potential μ with $\Delta = 0.1$ in the presence of uniform magnetic fields ($N = 8, M = 8$). At $\mu = 0$ the system lies in a topologically trivial phase. As μ increases, we observe successive gap closings at symmetry points Γ, Y, X, and M. Each gap closing accompanies a unit change in $\mathcal{N}$, and accordingly the system is expected to exhibit two TSC phases, one between the gap closings at Γ and Y and the other between those at X and M. The numerical computation of $\mathcal{N}$ reveals that the former corresponds to $\mathcal{N} = -1$ and the latter to $\mathcal{N} = 1$. After the last gap closing at M, the SC Chern number is 2, corresponding to $\mathcal{C} = 1$ QH state.

We numerically evaluate the SC Chern number together with the gap closing momenta in a wide region of (Δ, μ). The resulting phase diagram of SC Chern number as a function of the Fermi energy μ and SC gap Δ is shown in Fig. 3 for $N = M$ (uniform B) as well as $N \neq M$ (non-uniform B). The regions of even $\mathcal{N}$, indicated by hashes, are adiabatically connected, and thus
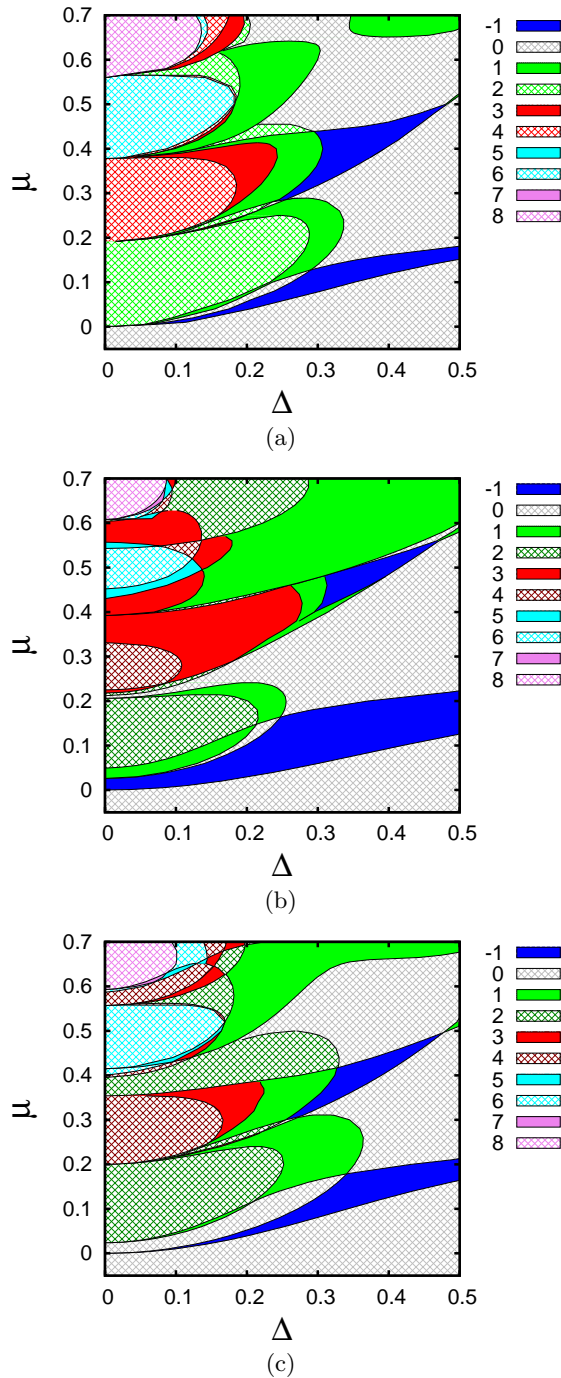
(a)

(b)

(c)

FIG. 3. Phase diagram of states for various geometries. Each phase is characterized by its Chern number $\mathcal{N}$, with different Chern numbers shown in different colors. The gray hashed region is an insulator; the colored hashed regions represent even integer $\mathcal{N}$, which correspond to QH effect; and the solid colors depict the topological superconductor phase with odd Chern numbers. The different panels show: (a) a uniform magnetic field ($N = 8, M = 8$), (b) a non-uniform periodic magnetic field of a square shape ($N = 8, M = 6$), and (c) a non-uniform magnetic field in stripe geometry ($N = 8, M = 6$).

equivalent, to conventional QH states with filling factor $\mathcal{C} = \frac{\mathcal{N}}{2}$. The regions with solid colors depict SC states with odd integer values of $\mathcal{N}$, i.e. the TSC phase. We also find narrow regions of semi-metallic phase near the phase boundaries where $\mathcal{N}$ changes by 2. These regions are discussed in App. B, but suppressed in Fig. 3 to avoid clutter.

It is evident that the phase diagram is very sensitive to how the magnetic field penetrates the superconductor. For a uniform magnetic field (Fig. 3a), only even values of $\mathcal{N}$ appear in the limit of weak SC gap $\Delta/t \to 0$, although TSC phases with an odd $\mathcal{N}$ can occur when Δ is sufficiently large. The same is true of the stripe geometry (Fig. 3c). As discussed in App. D, a hexagonal lattice of $h/2e$ fluxoids is also not effective in producing TSC. In striking contrast, for the non-uniform magnetic field produced by a square lattice of h/e fluxoids, TSC phases can emerge even in the limit $\Delta/t \to 0$, as shown by the blue, red and dark green areas in Fig. 3b. This property is also shared by a hexagonal lattice of h/e fluxoids (see App. E). We thus conclude that a square or a hexagonal lattice of h/e fluxoids is the best geometry for generating TSC. In App. F we also discuss coupling to p_x superconductivity and find that many of the above conclusions remain valid.

IV. DISCUSSION AND CONCLUSION

Mong et al.[40] considered stripes of QH states with their oppositely moving chiral edge states coupled by SC coupling or tunneling, and demonstrated emergence of TSC for certain parameters. While our work is in a topological sense similar, our model does not have edge states, and both QH effect and superconductivity coexist throughout the entire sample. Our study also allows high filling factors, thereby producing a rich phase diagram. Our model suggests that TSC phases can generally exist in QH-SC hybrid, without requiring fine-tuning of the parameters, provided the magnetic field has periodic spatial variation.

While a concrete calculation is needed to determine the most favorable geometries, it is possible to gain some intuitive insight into this question by noting that the TSC often occurs after a single Dirac type of transition that changes the SC Chern number by 1. For quasi-1D stripe geometry, such transitions are rare because the band is still flat along one direction. For fractional fluxoids, degeneracy can exist in the magnetic Brillouin zone and, in general, multiple Dirac transitions occur simultaneously, thus complicating the matter.

Before ending the article, it would be appropriate to mention important experimental recent progress in coupling the QH and SC phases. Supercurrent and Josephson coupling in QH regime at graphene-superconductor interface have been demonstrated at relatively low magnetic field ($\sim$ 2T)[33–35]. In another work, superconducting niobium nitride (NbN) electrode with very high crit-

ical magnetic field has been used to induce supercon-
ducting correlations in the QH edge states of graphene
to see evidence of crossed Andreev reflection on a QH
plateau[36]. In yet another work, inter-Landau level An-
dreev reflection has been observed in graphene coupled
to an NbSe$_2$ superconductor[37]. While the superconduc-
tor contains spin singlet Cooper pairs, it is in principle
possible to induce spin triplet superconductivity by ex-
ploiting spin-orbit coupling or inhomogeneous magneti-
zation at the interface. Such phenomena have been stud-
ied in a variety of hybrid systems with SC and magnetic
or strong spin-orbit coupled materials[41–44]. The feasibil-
ity to implement such mechanism in QH-SC hybrid will
be addressed in a future work. It should be possible to
construct a variety of QH-TSC planar junctions[27,32,45,46]
where the chemical potential may be controlled through
local gates. One advantage is the possibility of achieving
the TSC phase with $\mathcal{N} > 1$ in junction structures, which
has theoretically been proposed to give rise to unique
transport signature[45] that can unambiguously establish
chiral Majorana transport.

In summary, we have identified optimal conditions for
producing a topological superconductor by studying cou-
pling between QH effect and superconductivity in a mi-
croscopic model. We find that a non-uniform magnetic
field produced by a square or a hexagonal lattice of h/e
fluxoids is likely the best geometry for this purpose.

V. ACKNOWLEDGEMENT

Appendix A: Matrix Elements of BdG Hamiltonian

We give here the detailed form of the BdG Hamilto-
nian for a 2D electron gas in a magnetic field. With the
Fourier transform $c_{\boldsymbol{i}} = \frac{1}{L}\sum_{\boldsymbol{k}} e^{i\boldsymbol{k}\cdot\boldsymbol{R}_{\boldsymbol{i}}} c_{\boldsymbol{k},\tilde{\boldsymbol{r}}_i}$, where $|k_x| \le \pi/a, |k_y| \le \pi/a$, we obtain the Hamiltonian in the BdG
form

$$\mathcal{H} = \sum_{\boldsymbol{k}} \boldsymbol{C}_{\boldsymbol{k}}^{\dagger} \boldsymbol{H}_{\boldsymbol{k}} \boldsymbol{C}_{\boldsymbol{k}},$$

$$\boldsymbol{H}_{\boldsymbol{k}} = \begin{pmatrix} \boldsymbol{T}_{\boldsymbol{k}} & \boldsymbol{\Delta}_{\boldsymbol{k}}^{\dagger} \\ \boldsymbol{\Delta}_{\boldsymbol{k}} & -\boldsymbol{T}_{-\boldsymbol{k}}^{\dagger} \end{pmatrix} \qquad (A1)$$

where $\boldsymbol{C}_{\boldsymbol{k}}^{\dagger} = (c_{\boldsymbol{k},\tilde{\boldsymbol{r}}_1}^{\dagger}, \dots, c_{-\boldsymbol{k},\tilde{\boldsymbol{r}}_1}, \dots)$. The nonzero diago-
nal and off-diagonal terms in the above BdG Hamiltonian

are

$$(\boldsymbol{T}_{\boldsymbol{k}})_{\tilde{\boldsymbol{r}},\tilde{\boldsymbol{r}}'} = \begin{cases} -\mu & \text{for } \tilde{\boldsymbol{r}}' = \tilde{\boldsymbol{r}} \\ -te^{iA_{\tilde{\boldsymbol{r}},\tilde{\boldsymbol{r}}'}} & \text{for } \tilde{\boldsymbol{r}}' = \tilde{\boldsymbol{r}} + a_1\hat{x}, \tilde{\boldsymbol{r}} + a_1\hat{y} \\ -te^{i(A_{\tilde{\boldsymbol{r}},\tilde{\boldsymbol{r}}'}+k_x a)} & \text{for } \tilde{\boldsymbol{r}}' = \tilde{\boldsymbol{r}} - (N-1)a_1\hat{x} \\ -te^{i(A_{\tilde{\boldsymbol{r}},\tilde{\boldsymbol{r}}'}+k_y a)} & \text{for } \tilde{\boldsymbol{r}}' = \tilde{\boldsymbol{r}} - (N-1)a_1\hat{y} \end{cases}$$
$$(A2)$$

$$(\boldsymbol{\Delta}_{\boldsymbol{k}})_{\tilde{\boldsymbol{r}},\tilde{\boldsymbol{r}}'} = \begin{cases} -\Delta & \text{for } \tilde{\boldsymbol{r}}' = \tilde{\boldsymbol{r}} + a_1\hat{x} \text{ or } \tilde{\boldsymbol{r}} + a_1\hat{y} \\ -\Delta e^{ik_x a} & \text{for } \tilde{\boldsymbol{r}}' = \tilde{\boldsymbol{r}} - (N-1)a_1\hat{x} \\ -\Delta e^{ik_y a} & \text{for } \tilde{\boldsymbol{r}}' = \tilde{\boldsymbol{r}} - (N-1)a_1\hat{y} \end{cases}$$
$$(A3)$$

and their transposed elements given by $(\boldsymbol{T}_{\boldsymbol{k}})_{\tilde{\boldsymbol{r}}',\tilde{\boldsymbol{r}}} = (\boldsymbol{T}_{\boldsymbol{k}})_{\tilde{\boldsymbol{r}},\tilde{\boldsymbol{r}}'}^*$ and $(\boldsymbol{\Delta}_{\boldsymbol{k}})_{\tilde{\boldsymbol{r}}',\tilde{\boldsymbol{r}}} = -(\boldsymbol{\Delta}_{\boldsymbol{k}})_{\tilde{\boldsymbol{r}},\tilde{\boldsymbol{r}}'}^*$.

Appendix B: Certain general properties of the phase diagrams

In our calculated phase diagrams, the SC Chern num-
ber $\mathcal{N}$ generally decreases, going through successive tran-
sitions, as Δ is increased. Thus, conventional quantum
Hall states with high $\mathcal{N}$, which exist for small Δ, are
transformed to a trivial superconductor with $\mathcal{N} = 0$,
which is expected to occur at extremely large Δ.

Whether $\mathcal{N}$ changes by one or two depends on whether
the gap closes at one of the symmetry points or not. $\mathcal{N}$
changes by one when an energy gap closes at one of the
symmetry points. Otherwise, $\mathcal{N}$ changes by two because
the gap closes simultaneously at two different momenta
$\boldsymbol{k}_o$ and $-\boldsymbol{k}_o$, where $\boldsymbol{k}_o$ lies away from any high symmetry
momentum. Figure 4(a) shows an example of gap closing
at momenta that do not lie at symmetry points for $\mu = 0.38$ and $\Delta = 0.243$ with $N = M = 8$. On this boundary
the system undergoes a transition from $\mathcal{N} = 3$ to $\mathcal{N} = 1$.

When the SC Chern number $\mathcal{N}$ changes by one at
high symmetry momentum, the gap closing always oc-
curs at the chemical potential. However, when the SC
Chern number $\mathcal{N}$ changes by two, the energy gap does
not close exactly at the Fermi level, due to the absence of
both time reversal and inversion symmetries in our model
Hamiltonian. As shown in Fig. 4(b), the gap closes at an
energy slightly higher than the Fermi level ($E > 0$) at
one momentum $\boldsymbol{k}_o$ while slightly below the Fermi energy
($E < 0$) at the opposite momentum $-\boldsymbol{k}_o$. This indicates
that there exists, in some parameter regions on either
side of the phase boundary, a semi-metallic phase with
hole and electron pockets at two opposite momenta, al-
though two bands close to the Fermi level do not touch
each other. (As noted in the main text, we have de-
fined the SC Chern number with respect to half of the
bands in the BdG formalism, rather than with respect to
occupied states below the chemical potential. The two
definitions are identical when the chemical potential lies
inside a gap, but not when the chemical potential crosses
a band. In the semi-metallic region, while we find an
integer value for $\mathcal{N}$ with our definition, this value does
not correspond to a physically measurable transport co-
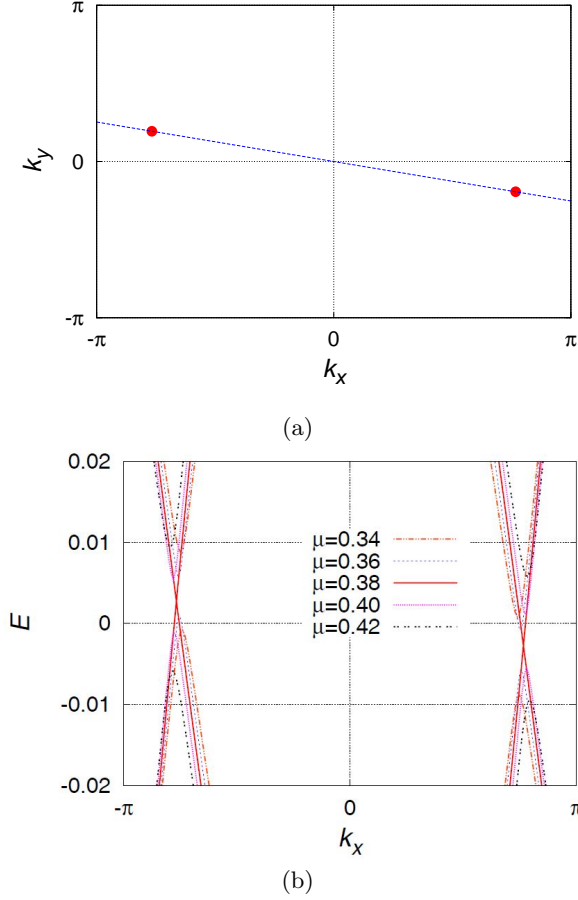efficient.) The semi-metallic regions are often small and

(a)

(b)

FIG. 4. (a) When a gap closes at a momentum $\boldsymbol{k}_o$ that does not lie at a symmetry point, the energy dispersion at $-\boldsymbol{k}_o$ also undergoes simultaneous gap closing. Consequently, Chern number changes by two on the phase boundary. The two red solid circles indicate the two momenta $\boldsymbol{k}_o$ and $-\boldsymbol{k}_o$ where the electron and the hole bands touch simultaneously for $\mu = 0.38$ and $\Delta = 0.243$ with $N = M = 8$. (b) The energy dispersions along the blue dashed line in (a) for $\Delta = 0.243$ and several values of μ with $N = M = 8$. The semi-metal phase with electron and hole pockets occurs at $\mu = 0.38$ (which is the phase boundary where $\mathcal{N}$ changes by 2) and $\mu = 0.36$.

were omitted in the phase diagrams shown in the main text to avoid distraction from the physics of TSC. For completeness, in Figs. 5 (a) and (b), the semi-metallic regions are demonstrated by the black thick closed lines.

Appendix C: Continuum Limit

We discuss the effects of a finite number N of lattice in a unit cell. The number of lattice points in a unit cell is N^2, which produces N^2 bands in the finite energy windows $4t$. We fix the magnetic flux in one unit-cell to be one flux quantum while varying N. The correct continuum limit is expected to maintain the constant spacing between Landau levels in the scaled energy of $N^2 E$. Fig-
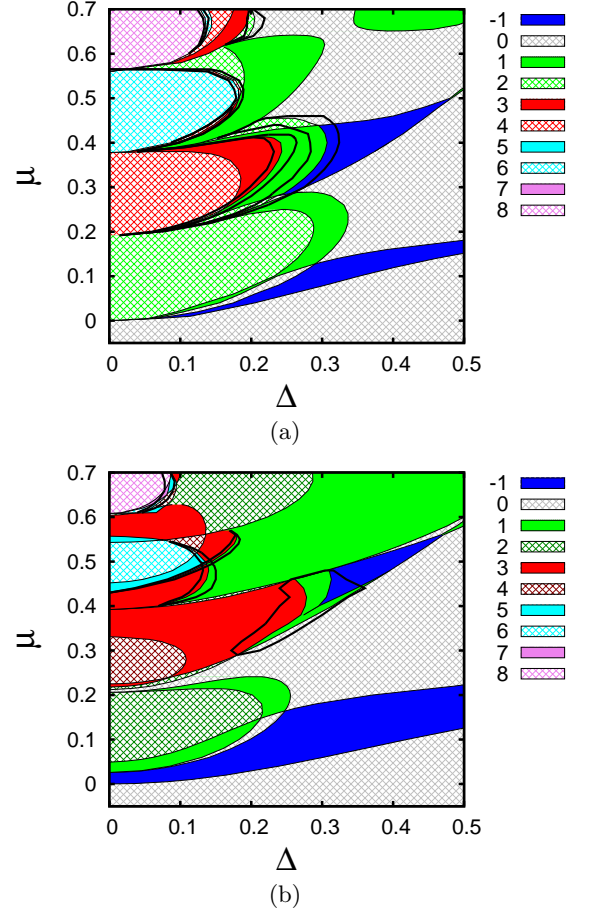

(a)

(b)

FIG. 5. Phase diagram under (a) uniform magnetic field ($N = 8, M = 8$); (b) non-uniform magnetic field ($N = 8, M = 6$). On the boundary when Chern number changes by two, we observe a semi-metallic phase on the finite region, which is displayed by black thick solid lines.

ure 6(a) demonstrates that the scaled energy measured from the minimum of the lowest band almost the same Landau level spacing for different N. The first few lowest levels exhibit essentially the same scaled energy even for $N = 8$. Although some quantitative deviation occurs for higher levels, they also saturate as N is increased.

In the presence of a nonuniform magnetic field, the scaled energies display similar saturations with the increase of N. In particular, the system with $N = 8$ already captures the essential features of the dispersive bands of the continuum limit.

One may suspect that the phase boundaries are also close to the thermodynamic limit. To explicitly demonstrate that, in Fig. 7 we plot the boundaries for the topological phases for $N = 8, 16, 32$. It turns out that when plotted as a function of $N\Delta$ as well as $N^2 E$, we obtain a collapse of the phase boundaries for small Δ, which is the region of maximum interest to us. As Δ is increased, the phase boundaries for different N begin to deviate, but still capture the thermodynamic phase diagram qualitatively and semiquantitatively.
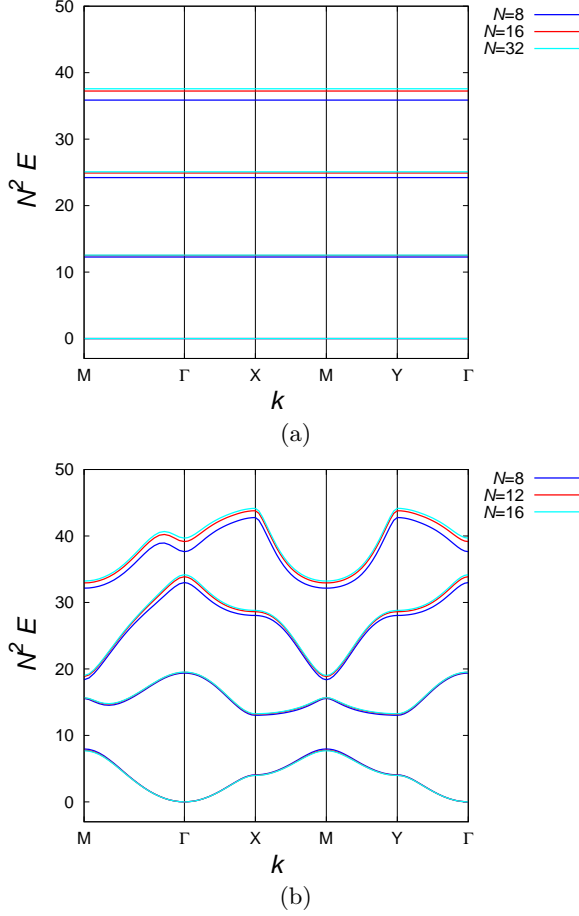
FIG. 6. Scaled energy dispersion N^2E for $N = 8, 16, 32$ under (a) uniform magnetic field ($N = M$); (b) non-uniform magnetic field ($M/N = 3/4$).
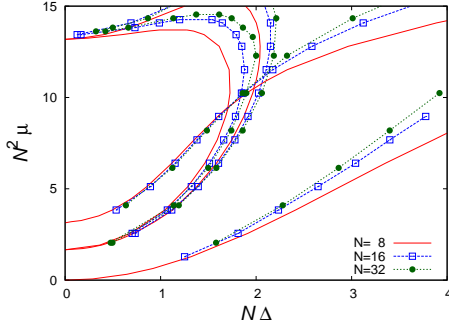

FIG. 7. Phase diagram in the plane of scaled chemical potential $N^2\mu$ and scaled SC pairing parameter $N\Delta$ for $N = 8, 16, 32$ under non-uniform magnetic field ($M/N = 3/4$).

Appendix D: periodic $h/2e$ fluxoids of a hexagonal shape in triangular lattice

We have also performed numerical calculations to obtain the phase diagram for a hexagonal Abrikosov lattice of $h/2e$ fluxoids. We use the same form of full

Hamiltonian as in the main text. The lattice points are arranged on the triangular lattice as shown in Fig. 8(a), and the nearest-neighbor vectors $\boldsymbol{\delta}_{1,2,3} = (1,0), (1/2, \sqrt{3}/2), (-1/2, \sqrt{3}/2)$ and the primitive lattice vectors can be chosen as $\mathbf{a}_1 = \boldsymbol{\delta}_1 = (1,0)$ and $\mathbf{a}_2 = \boldsymbol{\delta}_2 = (1/2, \sqrt{3}/2)$ on the cartesian coordinate. In an Abrikosov lattice of $h/2e$ fluxoids, one (magnetic) unit cell contains two $h/2e$ fluxoids (see Fig. 8(a)). Similar to square lattice, the lattice site in this triangular lattice can be labelled as $\boldsymbol{r}_{\boldsymbol{i}=(i_1,i_2)} = \boldsymbol{R}_{\boldsymbol{m}=(m_1,m_2)} + \tilde{\boldsymbol{r}}_{\boldsymbol{l}=(l_1,l_2)}$ for $(i_1, i_2) = (Nm_1 + l_1, 2Nm_2 + l_2)$ with $0 \le l_1 < N$, $0 \le l_2 < 2N$, $0 \le m_{1/2} < L$, and La and $2La$ being the linear dimensions of the system along the $\mathbf{a}_1$ and $\mathbf{a}_2$ directions, respectively. On the basis of $\mathbf{a}_1$ and $\mathbf{a}_2$, the lattice vector $\boldsymbol{r}_{\boldsymbol{i}=(i_x,i_y)}$ can be expressed as $\boldsymbol{r}_{\boldsymbol{i}=(i_1,i_2)} = i_1\mathbf{a}_1 + i_2\mathbf{a}_2$.

The resulting phase diagram in Fig. 8(b) reveals that there is no topological superconductor in the limit of $\Delta \to 0$. The TSC shows up for rather large Δ in the limited region. As in the square lattice, the TSC and normal superconductors are separated by the gap closing at the symmetry points, and two-fold gap-closing boundaries are also existing.

The absence of TSC phase in the $\Delta \to 0$ limit originates from an additional fundamental symmetry of $h/2e$ fluxoid lattice, which we analyze below. The Hamiltonian $\mathcal{H}$ still takes the form of Eq. (1) in the main text, but with $\mathbf{j}, \boldsymbol{\delta}$ defined on the triangle lattice. For convenience, we separate $\mathcal{H}$ into two parts, $\mathcal{H} = \mathcal{H}_0 + \mathcal{H}_\Delta$ where $\mathcal{H}_0$ includes the terms with the hopping parameter t and the chemical potential μ and $\mathcal{H}_\Delta$ includes the terms with pairing parameter Δ. We first focus on the single-particle Hamiltonian $\mathcal{H}_0$ and note that there are three terms in $\mathcal{H}_0$, which describes the hopping in three directions, described by $\boldsymbol{\delta}_1 = (1,0)$, $\boldsymbol{\delta}_2 = (0,1)$ and $\boldsymbol{\delta}_3 = (-1,1)$ on the basis of $\mathbf{a}_1$ and $\mathbf{a}_2$. This is different from the square lattice, which only has hopping along two directions. The Hamiltonian $\mathcal{H}_0$ is invariant under the following magnetic translation operators

$$\hat{T}_1 = \sum_{\boldsymbol{j}} c^\dagger_{\boldsymbol{j}+\boldsymbol{\tau}_1} c_{\boldsymbol{j}} e^{i \sum_{l_1} \chi_{\boldsymbol{j}+\boldsymbol{l}_1+\boldsymbol{\delta}_1, \boldsymbol{j}+\boldsymbol{l}_1}},$$

$$\hat{T}_2 = \sum_{\boldsymbol{j}} c^\dagger_{\boldsymbol{j}+\boldsymbol{\tau}_2} c_{\boldsymbol{j}} e^{i \sum_{l_2} \chi_{\boldsymbol{j}+\boldsymbol{l}_2+\boldsymbol{\delta}_2, \boldsymbol{j}+\boldsymbol{l}_2}}, \qquad \text{(D1)}$$

where $\boldsymbol{j} = (j_1, j_2)$ with the integers j_1, j_2, $\boldsymbol{\tau}_1 = (N, 0)$, $\boldsymbol{\tau}_2 = (0, N)$, $\boldsymbol{\delta}_1 = (1, 0)$, $\boldsymbol{\delta}_2 = (0, 1)$, $\boldsymbol{l}_1 = (l_1, 0)$ with the integer $0 \le l_1 < N - 1$, and $\boldsymbol{l}_2 = (0, l_2)$ with $0 \le l_2 < N - 1$. Here all the vectors are defined on the basis of $\mathbf{a}_1$ and $\mathbf{a}_2$. It should be noted that $\boldsymbol{\tau}_1$ is the translation of one magnetic unit cell along the $\mathbf{a}_1$ direction while $\boldsymbol{\tau}_2$ is the translation over *half* magnetic unit cell along the $\mathbf{a}_2$ direction (see Fig. 8(a)) The phase factor field $\chi_{\boldsymbol{j}+\boldsymbol{\delta}, \boldsymbol{j}}$ is defined on each bond of the lattice and can be determined
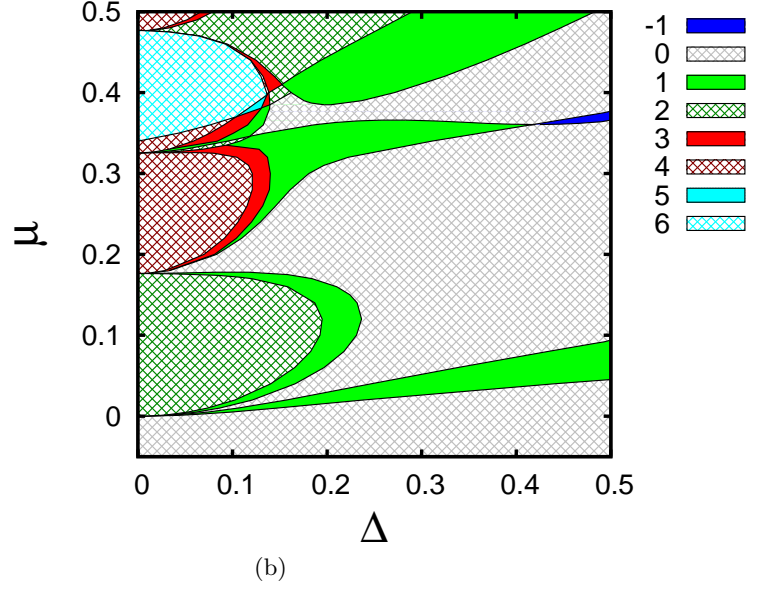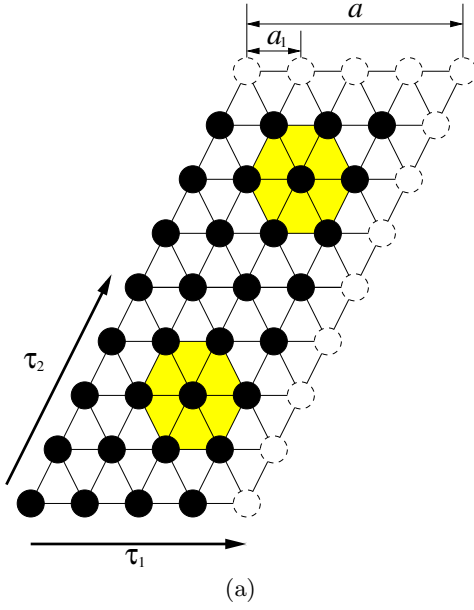
FIG. 8. (a) Schematic of a unit cell, and (b) phase diagram for a triangular lattice of $h/2e$ fluxoids of hexagonal shape ($N = 8, M = 6$). One unit cell is composed of $N \times 2N$ lattice points and two $h/2e$ fluxoids in hexagonally shaped yellow-shaded regions. The figure in (a) is an example of $N = 4$ and $M = 2$.
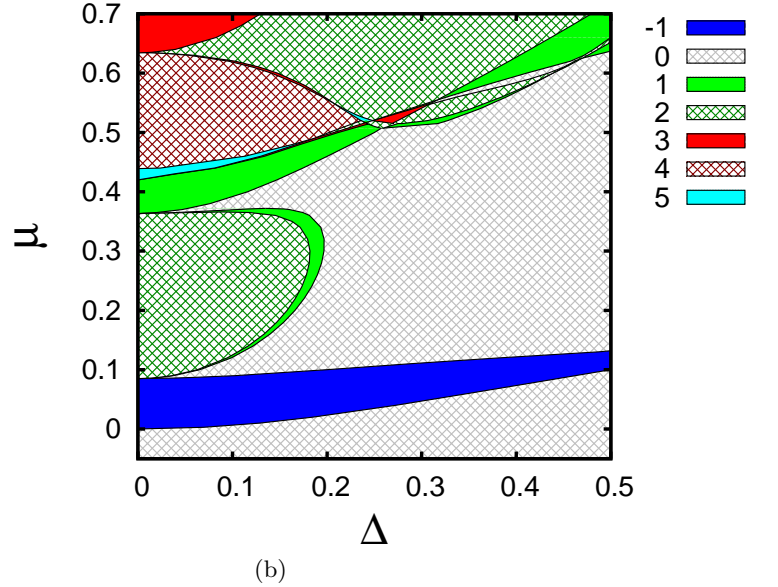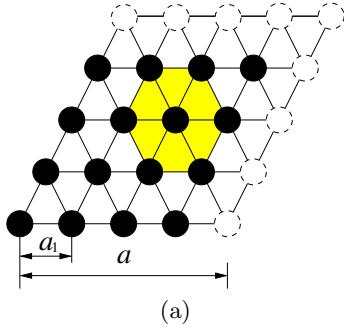

FIG. 9. (a) Schematic of a unit cell and (b) phase diagram under periodic h/e fluxoids of hexagonal shape ($N = 8, M = 6$) in triangular lattice. One unit cell is composed of $N \times N$ lattice points and a yellow-shaded zone of hexagon shape with $3M^2/2$ triangles contain h/e fluxoids. The figure in (a) is an example of $N = 4$ and $M = 2$.

by the vector potential field $A_{\boldsymbol{j}+\boldsymbol{\delta},\boldsymbol{j}}$ as

$$\nabla_1 \chi_{\boldsymbol{j}+\boldsymbol{\delta}_1,\boldsymbol{j}} = \nabla_1 A_{\boldsymbol{j}+\boldsymbol{\delta}_1,\boldsymbol{j}}, \tag{D2}$$

$$\nabla_2 \chi_{\boldsymbol{j}+\boldsymbol{\delta}_1,\boldsymbol{j}} = \nabla_1 A_{\boldsymbol{j}+\boldsymbol{\delta}_2,\boldsymbol{j}} = \nabla_2 A_{\boldsymbol{j}+\boldsymbol{\delta}_1,\boldsymbol{j}} + 2\pi\phi_{\boldsymbol{j}}, \tag{D3}$$

$$\nabla_2 \chi_{\boldsymbol{j}+\boldsymbol{\delta}_2,\boldsymbol{j}} = \nabla_2 A_{\boldsymbol{j}+\boldsymbol{\delta}_2,\boldsymbol{j}}, \tag{D4}$$

$$\nabla_1 \chi_{\boldsymbol{j}+\boldsymbol{\delta}_2,\boldsymbol{j}} = \nabla_2 A_{\boldsymbol{j}+\boldsymbol{\delta}_1,\boldsymbol{j}} = \nabla_1 A_{\boldsymbol{j}+\boldsymbol{\delta}_2,\boldsymbol{j}} - 2\pi\phi_{\boldsymbol{j}}. \tag{D5}$$

Here the discrete differential operator ∇ is defined as $\nabla_a f_{\boldsymbol{j}+\boldsymbol{\delta}_b,\boldsymbol{j}} = f_{\boldsymbol{j}+\boldsymbol{\delta}_b+\boldsymbol{\delta}_a,\boldsymbol{j}+\boldsymbol{\delta}_a} - f_{\boldsymbol{j}+\boldsymbol{\delta}_b,\boldsymbol{j}}$ with $a, b = 1, 2$

and $f = \chi, A$, and $2\pi\phi_{\boldsymbol{j}} = \nabla_1 A_{\boldsymbol{j}+\boldsymbol{\delta}_2,\boldsymbol{j}} - \nabla_2 A_{\boldsymbol{j}+\boldsymbol{\delta}_1,\boldsymbol{j}} = A_{\boldsymbol{j}+\boldsymbol{\delta}_2+\boldsymbol{\delta}_1,\boldsymbol{j}+\boldsymbol{\delta}_1} - A_{\boldsymbol{j}+\boldsymbol{\delta}_2,\boldsymbol{j}} - A_{\boldsymbol{j}+\boldsymbol{\delta}_1+\boldsymbol{\delta}_2,\boldsymbol{j}+\boldsymbol{\delta}_2} + A_{\boldsymbol{j}+\boldsymbol{\delta}_1,\boldsymbol{j}}$ labels the flux in the plaquette of the rhomboid formed by four sites $\boldsymbol{j}$, $\boldsymbol{j} + \boldsymbol{\delta}_1$, $\boldsymbol{j} + \boldsymbol{\delta}_2$ and $\boldsymbol{j} + \boldsymbol{\delta}_1 + \boldsymbol{\delta}_2$. Here the flux $\phi_{\boldsymbol{j}}$ satisfies the periodic conditions $\phi_{\boldsymbol{j}} = \phi_{\boldsymbol{j}+\boldsymbol{\tau}_a}$ with $a = 1, 2$ and $\sum_{\boldsymbol{j}} \phi_{\boldsymbol{j}} = 1/2$ where the summation over $\boldsymbol{j} = (j_1, j_2)$ is within the range $0 \leq j_{1,2} < N$. The phase factor $\chi_{\boldsymbol{j}+\boldsymbol{\delta}_1,\boldsymbol{j}}$ ($\chi_{\boldsymbol{j}+\boldsymbol{\delta}_2,\boldsymbol{j}}$) determined by D2 and D3

(D4 and D5) will make the operator $\hat{T}_1$ ($\hat{T}_2$) commutate with the hopping terms along the $\boldsymbol{\delta}_1$ and $\boldsymbol{\delta}_2$ directions in $\mathcal{H}_0$, which is similar to the case of a square lattice under magnetic fields[47]. For the hopping along the $\boldsymbol{\delta}_3$ direction, one can still show its commutation with $\hat{T}_a$ due to the periodic condition $\phi_{\boldsymbol{j}} = \phi_{\boldsymbol{j}+\boldsymbol{\tau}_a}$ after some length derivation. Therefore, $\hat{T}_a$ defines the magnetic translation ($[\hat{T}_a, \mathcal{H}_0] = 0, a = 1, 2$) for our system. In addition, since the rhomboid formed by two vectors $\boldsymbol{\tau}_1$ and $\boldsymbol{\tau}_2$ encloses half flux quantum for our $h/2e$ fluxoid lattice, we find the anti-commutation relation $\{\hat{T}_1, \hat{T}_2\} = 0$ within the single-particle Hilbert space. These commutation or anti-commutation relations within the operation sets of $\hat{T}_1$, $\hat{T}_2$ and $\mathcal{H}_0$ determine the energy spectrum of the Abrikosov lattice system.

The eigenstate $|\boldsymbol{k}\rangle$ of the Hamiltonian $\mathcal{H}_0$ can be chosen as $\mathcal{H}_0|\boldsymbol{k}\rangle = E(\boldsymbol{k})|\boldsymbol{k}\rangle$, $\hat{T}_1|\boldsymbol{k}\rangle = e^{ik_1}|\boldsymbol{k}\rangle$ and $\hat{T}_1^2|\boldsymbol{k}\rangle = e^{i2k_2}|\boldsymbol{k}\rangle$ with $\boldsymbol{k} = (k_1, k_2)$ since $\mathcal{H}_0$, $\hat{T}_1$ and $\hat{T}_2^2$ all commutate with each other. Here k_1 and k_2 are continuous variables in the range $-\pi \leq k_1 < \pi$ and $-\pi/2 \leq k_2 < \pi/2$. Let us consider two eigenstates $|\boldsymbol{k}\rangle$ and $\hat{T}_2|\boldsymbol{k}\rangle$ and it is clear that these two eigenstates share the same eigenenergy since $[\mathcal{H}_0, \hat{T}_2] = 0$. Due to the anti-commutation between $\hat{T}_1$ and $\hat{T}_2$, we find $\hat{T}_1\hat{T}_2|\boldsymbol{k}\rangle = -\hat{T}_2\hat{T}_1|\boldsymbol{k}\rangle = -e^{ik_1}\hat{T}_2|\boldsymbol{k}\rangle = e^{i(k_1+\pi)}\hat{T}_2|\boldsymbol{k}\rangle$. This suggests that $\hat{T}_2|\boldsymbol{k}\rangle \sim |\boldsymbol{k} + (\pi, 0)\rangle$ and all the eigenstates at $\boldsymbol{k}$ and $\boldsymbol{k} + (\pi, 0)$ share the same energy spectrum. Based on this conclusion, one can see that Dirac type of topological phase transition must occur in pairs at $\boldsymbol{k}$ and $\boldsymbol{k} + (\pi, 0)$ in the entire Brillouin zone and thus the SC Chern number always changes by ± 2 in the $\Delta \to 0$ limit. This implies absence of TSC phase in this limit. This argument is not valid for a finite Δ, because the p-wave pairing term $\mathcal{H}_\Delta$ used in our calculations is *not* gauge invariant under magnetic translations $\hat{T}_{1,2}$. Therefore, the TSC phase can be present at a finite Δ.

Appendix E: periodic h/e fluxoids of a hexagonal shape in triangular lattice

We finally show the phase diagram for topological superconductors in the presence of a hexagonal lattice of h/e fluxoids. The lattice points are arranged on a triangular lattice as shown in Fig. 9(a), with the nearest-neighbor vectors given by $\boldsymbol{\delta} = (1, 0), (1/2, \sqrt{3}/2), (-1/2, \sqrt{3}/2)$. Each unit cell contains a single h/e fluxoid. This geometry also produces topological superconductors in the limit of $\Delta \to 0$, as demonstrated in Fig. 9(b). The TSC phases intervene between the adjacent normal quantum Hall phases, as was the case for periodic square fluxes.

Compared to the periodic $h/2e$ fluxoid lattice, the magnetic translation symmetry and the lattice translation in the periodic h/e fluxoid lattice coincide and thus do not produce any additional symmetry leading to degeneracy. As a result, the TSC phase is allowed in the limit $\Delta \to 0$.

Appendix F: Coupling to p_x or p_y superconductivity

In this section we ask how the phase diagram is modified if the p-wave superconductivity has p_x or p_y symmetry. The phase diagrams are shown in Fig. 10 for three cases. Two cases (a) and (b) correspond to when the magnetic field forms stripes along the x-direction and the superconductivity is either p_x or p_y. We find that topological superconductivity is strongly suppressed in the former case shown in (a), because the gap always closes in pairs of symmetry related points, but regions of topological superconductivity appear in the latter (b). For the third case, where the magnetic flux forms a lattice, coupling to p_x superconductivity again produces topological superconductivity for certain parameter range as seen in panel (c).

This study shows that the qualitative results of our study are not sensitive to the nature of the p-wave superconductivity. More detailed predictions can be deduced once the specific experimental geometry is known.
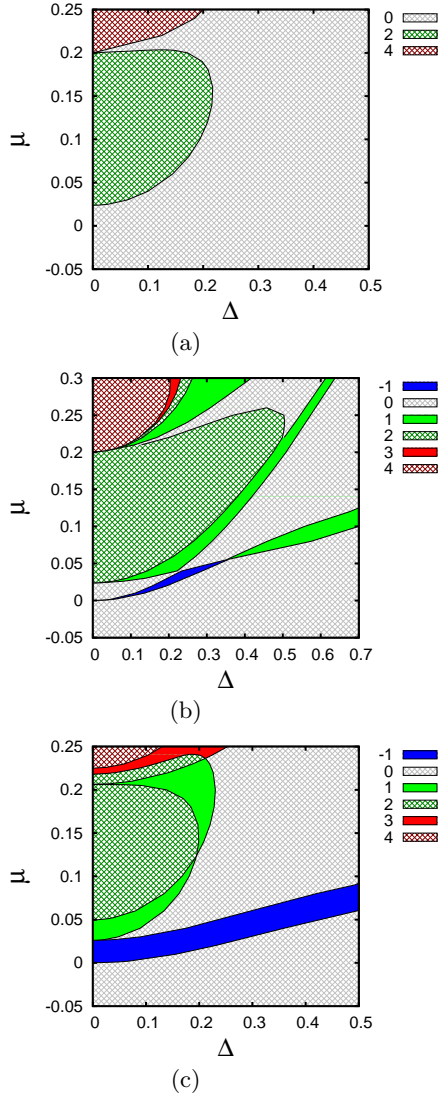
FIG. 10. The top panel (a) shows the phase diagram for a superconductor with p_x-wave pairing and the middle panel (b) with p_y-wave pairing, with the magnetic field configuration having stripes along the x direction ($N = 8, M = 6$). The bottom panel (c) shows the phase diagram for a square lattice of ϕ_0 flux ($N = 8, M = 6$) with p_x-wave pairing.

[1] A. Stern, Ann. Phys. **323**, 204 (2008).

[2] C. Nayak, S. H. Simon, A. Stern, M. Freedman, and S. Das Sarma, Rev. Mod. Phys. **80**, 1083 (2008).

[3] J. Alicea, Rep. Prog. Phys. **75**, 076501 (2012).

[4] C. Beenakker, Annu. Rev. Condens. Matter Phys. **4**, 113 (2013).

[5] A. Y. Kitaev, Physics-Uspekhi **44**, 131 (2001).

[6] A. Kitaev, Ann. Phys. **303**, 2 (2003).

[7] S. D. Sarma, M. Freedman, and C. Nayak, npj Quantum Information **1**, 15001 (2015).

[8] J. Alicea and A. Stern, Physica Scripta **2015**, 014006 (2015).

[9] N. Read and D. Green, Phys. Rev. B **61**, 10267 (2000).

[10] T. Rice and M. Sigrist, J. Phys.: Condens. Matter **7**, L643 (1995).

[11] V. Mourik, K. Zuo, S. M. Frolov, S. Plissard, E. P. Bakkers, and L. P. Kouwenhoven, Science **336**, 1003 (2012).

[12] A. Das, Y. Ronen, Y. Most, Y. Oreg, M. Heiblum, and H. Shtrikman, Nat. Phys. **8**, 887 (2012).

[13] L. P. Rokhinson, X. Liu, and J. K. Furdyna, Nat. Phys. **8**, 795 (2012).

[14] R. M. Lutchyn, J. D. Sau, and S. D. Sarma, Phys. Rev. Lett. **105**, 077001 (2010).

[15] J. D. Sau, R. M. Lutchyn, S. Tewari, and S. D. Sarma, Phys. Rev. Lett. **104**, 040502 (2010).

[16] J. Alicea, Phys. Rev. B **81**, 125318 (2010).

[17] J. Alicea, Y. Oreg, G. Refael, F. Von Oppen, and M. P. Fisher, Nat. Phys. **7**, 412 (2011).

[18] S. Nadj-Perge, I. K. Drozdov, J. Li, H. Chen, S. Jeon, J. Seo, A. H. MacDonald, B. A. Bernevig, and A. Yazdani, Science **346**, 602 (2014).

[19] L. Fu and C. L. Kane, Phys. Rev. Lett. **100**, 096407 (2008).

[20] J.-P. Xu, M.-X. Wang, Z. L. Liu, J.-F. Ge, X. Yang, C. Liu, Z. A. Xu, D. Guan, C. L. Gao, D. Qian, et al., Phys. Rev. Lett. **114**, 017001 (2015).

[21] M.-X. Wang, C. Liu, J.-P. Xu, F. Yang, L. Miao, M.-Y. Yao, C. Gao, C. Shen, X. Ma, X. Chen, et al., Science **336**, 52 (2012).

[22] J. Yin, Z. Wu, J. Wang, Z. Ye, J. Gong, X. Hou, L. Shan, A. Li, X. Liang, X. Wu, et al., Nat. Phys. **11**, 543 (2015).

[23] X. Wu, S. Qin, Y. Liang, H. Fan, and J. Hu, Phys. Rev. B **93**, 115129 (2016).

[24] P. Zhang, K. Yaji, T. Hashimoto, Y. Ota, T. Kondo, K. Okazaki, Z. Wang, J. Wen, G. Gu, H. Ding, et al., Science **360**, 182 (2018).

[25] Z. Wang, P. Zhang, G. Xu, L. Zeng, H. Miao, X. Xu, T. Qian, H. Weng, P. Richard, A. V. Fedorov, et al., Phys. Rev. B **92**, 115119 (2015).

[26] X.-L. Qi, T. L. Hughes, and S.-C. Zhang, Phys. Rev. B **82**, 184516 (2010).

[27] S. B. Chung, X.-L. Qi, J. Maciejko, and S.-C. Zhang, Phys. Rev. B **83**, 100512 (2011).

[28] Q. L. He, L. Pan, A. L. Stern, E. C. Burks, X. Che, G. Yin, J. Wang, B. Lian, Q. Zhou, E. S. Choi, et al., Science **357**, 294 (2017).

[29] B. Lian, J. Wang, X.-Q. Sun, A. Vaezi, and S.-C. Zhang, Phys. Rev. B **97**, 125408 (2018).

[30] W. Ji and X.-G. Wen, Phys. Rev. Lett. **120**, 107002 (2018).

[31] Y. Huang, F. Setiawan, and J. D. Sau, Phys. Rev. B **97**, 100501 (2018).

[32] B. Lian, X.-Q. Sun, A. Vaezi, X.-L. Qi, and S.-C. Zhang, PNAS **115**, 10938 (2018).

[33] P. Rickhaus, M. Weiss, L. Marot, and C. Schnenberger, Nano Lett. **12**, 1942 (2012).

[34] F. Amet, C. T. Ke, I. V. Borzenets, J. Wang, K. Watanabe, T. Taniguchi, R. S. Deacon, M. Yamamoto, Y. Bomze, S. Tarucha, et al., Science **352**, 966 (2016).

[35] M. Ben Shalom, M. J. Zhu, V. I. Fal'ko, A. Mishchenko, A. V. Kretinin, K. S. Novoselov, C. R. Woods, K. Watanabe, T. Taniguchi, A. K. Geim, et al., Nat. Phys. **12**, 318 (2016).

[36] G.-H. Lee, K.-F. Huang, D. K. Efetov, D. S. Wei, S. Hart, T. Taniguchi, K. Watanabe, A. Yacoby, and P. Kim, Nat. Phys. **13**, 693 (2017).

[37] M. R. Sahu, X. Liu, A. K. Paul, S. Das, P. Raychaudhuri, J. K. Jain, and A. Das, Phys. Rev. Lett. **121**, 086809 (2018).

[38] C.-Z. Chang, J. Zhang, X. Feng, J. Shen, Z. Zhang, M. Guo, K. Li, Y. Ou, P. Wei, L.-L. Wang, et al., Science **340**, 167 (2013).

[39] D. J. Thouless, M. Kohmoto, M. P. Nightingale, and M. den Nijs, Phys. Rev. Lett. **49**, 405 (1982).

[40] R. S. K. Mong, D. J. Clarke, J. Alicea, N. H. Lindner, P. Fendley, C. Nayak, Y. Oreg, A. Stern, E. Berg, K. Shtengel, et al., Phys. Rev. X **4**, 011036 (2014).

[41] A. I. Buzdin, Rev. Mod. Phys. **77**, 935 (2005).

[42] F. Bergeret, A. F. Volkov, and K. B. Efetov, Rev. Mod. Phys. **77**, 1321 (2005).

[43] M. Eschrig, Phys. Today **64**, 43 (2011).

[44] M. Eschrig, Rep. Prog. Phys. **78**, 104501 (2015).

[45] J. Wang and B. Lian, arXiv preprint arXiv:1805.10763 (2018).

[46] B. Lian, J. Wang, and S.-C. Zhang, Phys. Rev. B **93**, 161401 (2016).

[47] B. Bernevig and T. Hughes, Topological Insulators and Topological Superconductors (Princeton University Press, 2013).